

Unmanned F/A-18 Aircraft Landing Control on Aircraft Carrier in Adverse Conditions

Mikhail Kistyarev, Xinhua Wang
Aerospace Engineering, University of Nottingham, UK
Email: wangxinhua04@gmail.com

ABSTRACT

Carrier landings are a difficult control task due to wind disturbances and a changing trajectory. Demand for carrier-based drones is increasing. A robust and accurate landing control system is crucial to meet this demand. Control performance can be improved by using observers to estimate unknown variables and disturbances for feedback. This study applies a nonlinear observer to estimate the combined disturbance in the pitch dynamics of an F/A-18 during carrier landing. Additionally, controllers to regulate the velocity, rate of descent and vertical position are designed. A full model, including the nonlinear flight dynamics, controller, carrier deck motion, wind and measurement noise is modelled numerically and implemented in software. Combined with proportional derivative control, the proposed pitch control method is shown to be very effective converging 85% faster than a PID controller. The simulations, verify that the pitch controller can quickly track a time-varying reference despite noise and disturbances. The positional controller used is found to be ineffective and requires improvement.

1. INTRODUCTION

Carrier landings are considered to be the most challenging routine task of airplane operations [1] Mainly due to the small dimensions of the runway [1], carrier deck motion [1] and wind disturbances. Due to the complexity of carrier landings, navies must spend additional resources to rigorously train pilots and established autopilots are not robust enough to be used for carrier landings. Additionally, demand for carrier-based UAVs is increasing. For example, to fulfil the needs of longer endurance missions, 20-30% of US Navy's F/A-18 E/F fighter jet missions are refuelling ones [2]. This means that highly qualified fighter pilots are being utilised as tankers rather than focusing on their primary objectives [2]. Hence, Boeing are developing the MQ-25A Stingray, the world's first autonomous carrier-based aerial tanker [2] capable of autonomous air-to-air refuelling, which is currently in the testing and development phase. Even the MQ-25A requires landing assistance from the crew [2] with the chief engineer, Jim Youngs, saying "The biggest challenge is taking an unmanned vehicle and landing it on a moving runway" [2]. This highlights that a robust UAV control system capable of landing on an aircraft carrier is important to the development of carrier-based UAVs and a very current problem. Highly non-linear wind disturbances make it difficult for an aircraft to track a reference trajectory.

because they influence the aerodynamic forces and moments by varying the airspeed. This is especially true for a trajectory that is changing due to the carrier deck motion. Therefore, a method of rejecting the non-linear disturbance and adjusting the flight path is a crucial element of a robust carrier landing control system. Hence, the focus of this paper has investigated whether a non-linear observer developed by Wang et al [3] for use in quadrotor aircraft can be used to estimate a non-linear disturbance and reject noise in the carrier landing context. The observed disturbance estimate is used to design a controller for longitudinal pitch dynamics of and F/A-18. This controller is tested inside a complete carrier landing system model and verified in simulation.

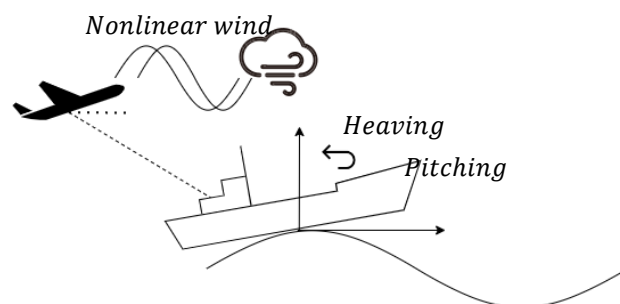


Figure 1 Simple schematic of carrier landing

2. BACKGROUND

2.1 Literature

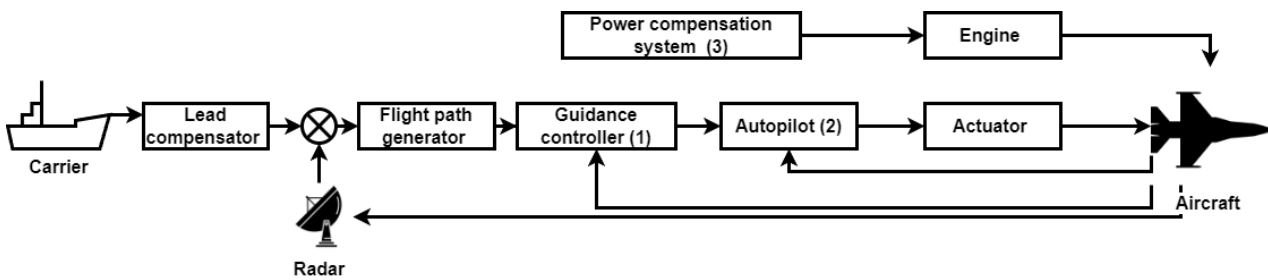


Figure 2 Typical carrier landing architecture

Most of the current research is still based around the original AN/SPN-42 automatic carrier landing system architecture shown in Figure 2. This system was based on a radar tracking the separation between the aircraft and carrier [4]. From this, position errors are calculated based on the aircraft's range, altitude and desired glide slope [4] which are filtered and passed through a PIDDD guidance controller [4]. This outputs pitch and roll commands to manoeuvre the aircraft to the required glide path [4]. The commands are implemented through the aircraft's Automatic Flight control system (AFCS) [4] (autopilot) which tracks the commands by setting the actuator signals. Additionally, an Automatic Power Compensation System (APCS) is used to maintain a reference angle of attack [4] by controlling the throttle. During most of the approach the aircraft is directed to the average touchdown position. However, during the last 12 seconds of landing, the aircraft begins to track the exact position of the touchdown position [4] by an additional altitude command to the vertical error [5] determined by using lead compensation added to the deck position measurement which predicts the future position of the touchdown point. Most modern papers have used the same architecture and focused on improving individual elements. [6] compare the effectiveness of 3 different guidance controllers for adjusting the flight path, based on PID, PIDDD and Fuzzy PID. They show the controllers to all be effective when no turbulence is present. However, they all fail when an aerodynamic disturbance is introduced, highlighting that an effective flight path controller is crucial. [4] investigated 3 different autopilot controllers' effectiveness at controlling the glide path with deck motion prediction. A conventional controller based on controlling the pitch using the elevators [4], conventional with a direct-lift controller

(DLC) which alters the sink rate based on using spoilers and flaps [4] and a conventional controller with DLC and thrust vectoring. [4] Concludes that the addition of DLC, provides better glide slope tracking precision due to the faster reaction to vertical displacement errors [4]. However, deck motion prediction is assumed to be completely accurate meaning that an accurate deck motion prediction method is needed before it can be implemented. [7] proposes landing risk model based on probability. This risk is used as a compensating state together with a nonlinear dynamic inversion-based autopilot and is shown to increase the rapidity and robustness of the control system. [8] proposed a method for tracking the required glide path based on sliding mode control. Using Monte-Carlo simulations for considering, various sea states and measurement delay, the proposed controller is shown to achieve successful landings in 95% of cases. [9] proposes an optimal preview control method-based track a desired trajectory which is corrected with carrier deck motion prediction from particle filtering algorithms which is shown to be more effective than PID and LQ controllers. [10] applies a similar method and finds the steady-state position error to be less than 0.14m under typical sea conditions. [11] Proposes an attitude controller based on active disturbance rejection control. Here a linear extended state observer is used to estimate all the internal and external disturbances in the pitch dynamics and combined with a linear controller. The results is shown to settle 82% faster than a PID controller and with less overshoot. A similar method is proposed in this study, where the linear controller is a proportional-derivative controller and the observer is a nonlinear observer discussed in 2.3.

2.2 Technical problems

Table 1 Nomenclature

	Name	Sym bol	Units
Constants	Aircraft mass	m	kg
	Air density	ρ	kgm^{-3}
	Acceleration due to gravity	g	ms^{-2}
	Maximum thrust	T_{max}	$kgms^{-2}$
	Aircraft surface area	S	m^2
	Aircraft moment of inertial around y-axis	J_y	kgm^2
	Mean aerodynamic chord	\bar{c}	m
Control Variables	Airspeed	V_T	ms^{-1}
	Inertial speed	V	ms^{-1}
	Pitch angle	θ	rad
	Angle of attack	α	rad
	Pitch rate	q	$rads^{-1}$
	Flight path angle	γ	rad
Control inputs	Elevator deflection	δ_e	$^\circ$
	Thrust	T	N
	Throttle	δ_T	-
Aerodynamic variables	Lift force	L	N
	Drag force	D	N
	Pitching moment	M	N
	Dynamic pressure	\bar{q}	Pa
	Wind speed	V_w	ms^{-1}

2.2.1 Non-linear flight dynamics

2.2.1.1 Equations of motion

The aircraft longitudinal plane is shown Figure 3 below with the variables and axis shown in black, the forces in red and the control inputs in blue. The longitudinal dynamics are governed by 4, coupled, first-order, implicit, non-linear differential equations shown in (1-4). These are well described and derived in [12]

$$\dot{V}_T = \frac{T \cos(\alpha)}{m} - \frac{D}{m} - g \sin(\gamma) \quad (1)$$

$$\dot{\theta} = q \quad (2)$$

$$\dot{\alpha} = -\frac{T \sin(\alpha)}{mV_T} - \frac{L}{mV_T} + g \cos(\gamma) \quad (3)$$

$$\dot{q} = \frac{M}{J_y} \quad (4)$$

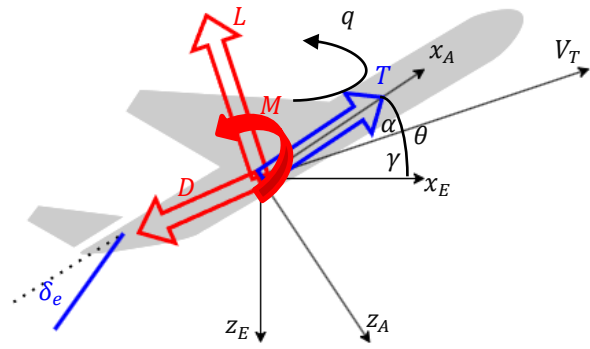


Figure 3 Aircraft longitudinal plane

2.2.1.2 Control inputs

The aircraft has 2 control inputs in the longitudinal plane: the elevator deflection and thrust. The elevator mainly affects the pitching moment which induces a pitch rate and hence a change in the pitch angle. Additionally, the elevator deflection causes minor changes in the drag and lift values. The thrust mainly affects the airspeed, especially at small angle of attacks.

2.2.1.3 Implications

The equations are non-linear; hence, linear control methodologies cannot be used directly. The equations must either decoupled and linearised or non-linear control methodologies must be used. The equations are under actuated, meaning there are some variables that cannot be controlled directly. For example, the vertical position must be controlled by changing the pitch via the elevator which induces a change in the trajectory.

2.2.2 Wind disturbance

A wind disturbance causes a change in the airspeed ($\vec{V}_T = \vec{V} - \vec{V}_w$) which changes the dynamic pressure. The aerodynamics forces and moments are directly proportional to the dynamic pressure as seen in Equation 5 and 6. Hence, wind disturbance cause fluctuations in the aerodynamic forces and alter the aircraft dynamics. These disruptions make it more difficult to control the aircraft and track required values.

$$\bar{q} = \frac{1}{2} \rho V_T^2 \quad (5) \quad L, D, M = \bar{q} S C_{L, D, M} \quad (6)$$

2.2.3 Carrier deck motion

Carrier deck motion changes the position of the landing point. Hence a constant trajectory cannot be used for approach. Instead, a sink

rate or position commands must be sent to the autopilot to track the carrier deck motion. These movement are caused by the sea waves and can be split into two motions in the longitudinal plane: a heaving(vertical) translational motion of the ships centre of mass and a pitching rotational motion around its centre of mass. This causes a combined planar motion in the landing position. The aircraft's trajectory must track this motion to land successfully.

2.2.4 Measurement noise

Measurement noise is the error between the actual and measured value of a variable. Often, it is in the form of a low-amplitude, high frequency wave or random stochastic disruption. This introduces uncertainties into the system and behaves like a disturbance. This makes it more difficult to track a reference value and increases actuator oscillations which dissipates energy.

2.3 Nonlinear Observer

A nonlinear augmented observer detailed in [3] will be used to estimate and compensate for the disturbance in the aircraft pitch dynamics. Observers are designed to estimate unknown variables by comparing the error between a measured output value and estimated value given known inputs. This error is used in a closed feedback loop to improve the accuracy of the estimate. These estimates can then be used by a controller to improve control performance or regulate unknowns.

This nonlinear observer is designed using the small perturbation method and is shown to be capable of synchronously estimating the first-derivative and disturbance of a measured output variable with finite-time stability and stochastic disturbance rejection. The observer must be applied to systems in the form shown below in equations 7-10, where w_1 represents the measured output variable y_{op} , $h(t)$ a known input and w_3 an unknown bounded disturbance with derivative $\eta(t)$.

$$\dot{w}_1 = w_2 \quad (7)$$

$$\dot{w}_2 = w_3 + h(t) \quad (8)$$

$$\dot{w}_3 = \eta(t) \quad (9)$$

$$y_{op} = w_1 \quad (10)$$

The observer is implemented using the form shown below in equations 11-13 where the x-variables x_1, x_2 and x_3 represent estimates of w_1, w_2 and w_3 respectively.

$$\dot{x}_1 = x_2 - \frac{k_3}{\varepsilon} |x_1 - y_{op}|^{\alpha_3} \text{sign}(x_1 - y_{op}) \quad (11)$$

$$\dot{x}_2 = x_3 - \frac{k_2}{\varepsilon^2} |x_1 - y_{op}|^{\alpha_2} \text{sign}(x_1 - y_{op}) \quad (12)$$

$$\dot{x}_{1,3} = -\frac{k_1}{\varepsilon^3} |x_1 - y_{op}|^{\alpha_3} \text{sign}(x_1 - y_{op}) \quad (13)$$

The parameters $\alpha_1, \alpha_2, \alpha_3, k_1, k_2, k_3$ and ε vary the system precision, stability and robustness and must be selected appropriately. Justifications and rules for selecting these parameters are rigorously explained and derived in [3] for the interested reader. However, the main conclusions are summarised below.

- k_1, k_2, k_3 must be selected such that $\{k_1, k_2, k_3 | k_1 > 0, k_3 > 0, k_2 > \frac{4k_1}{\pi k_3}\}$ so that the Routh-Hurwitz stability criterion is satisfied, and the observer is stable.
- Increasing α_1 improves the estimation precision. Where $\alpha_1 \in (0, 1)$, $\alpha_2 = \frac{2\alpha_1 + 1}{3}$ and $\alpha_3 = \frac{\alpha_1 + 2}{3}$
- Reducing ε where $\varepsilon \in (0, 1)$ increases the bandwidth of the observer hence higher frequency signals can be estimated. However, less noise is rejected.

3 METHODOLOGY

The control scheme will be verified in simulation. This section describes the numerical models used. Additionally, a brief description of the simulation method is provided.

3.1 Aircraft model

As mentioned, the longitudinal dynamics of an aircraft are governed by equations (1-4). The physical constants for the F/A-18 were obtained from [13] and are summarised in Table 2. Due to the low altitude range, the density is assumed to be constant as the airspeed fluctuations caused by the wind disturbance will dominate over the minor density changes with altitude.

Table 2 Constants

Symbol	Value	Units
m	15118.35	kg
ρ	1.225	kgm^{-3}
g	9.81	ms^{-2}
T_{max}	150000	$kgms^{-2}$
S	37.16	m^2

J_y	205113.07	kgm^2
\bar{c}	3.511	m

The aerodynamic forces are functions of the dynamic pressure and the aerodynamics coefficients C_L, C_D and C_M . The aerodynamic coefficients can be approximated as functions of the angle of attack, pitch rate and elevator deflection. These coefficients were obtained as a lookup table from an official NASA F/A-18 high angle of attack research model available at [14]. These are based on experimental data collected during test flights. These coefficients assume a clean no-flap configuration. However, during landing an F/A-18 would deploy flaps which would shift the C_L curve up by constant. This constant was estimated to be 0.7. The coefficients at δ_e and q set to zero are shown in Figure 4

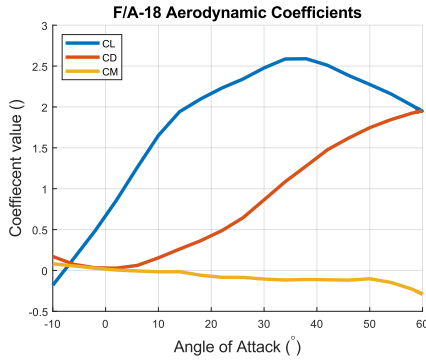


Figure 4 F/A-18 Aerodynamic coefficients

3.2 Linearised form

The observer estimates all the non-linearities in the pitch dynamics. Hence, linear control methods can be used to design the pitch controller. So, the equations of motion must be linearised around an equilibrium (trim) condition.

3.2.1 Equilibrium trim conditions

The trim conditions selected is steady level flight for the following reasons:

- The aircraft may need to climb or sink to track ship motion. The level position is the neutral position between climb and sink.
- The trim conditions are simple and trim values are easy to obtain.

The trim conditions (denoted by $*$) for steady level flight are detailed in [13] and well known to be.

$$L^* = mg, \quad T^* = D^*, \quad M^* = 0$$

Given the partial derivative of the aerodynamic coefficients with respect to the angle of attack $C_{L\alpha}, C_{D\alpha}$ and $C_{M\alpha}$ the trim variables are easy to obtain. However, the model used does not include these partial derivatives. Hence, they must be estimated. Therefore, the trim process

shown in Figure 5 includes an additional step where the aerodynamic coefficients and airspeed are updated to match the estimated α and δ_e values.

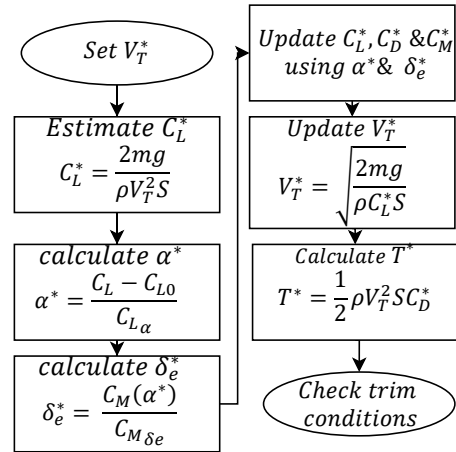


Figure 5 Trim flowchart

After trial and error, the aircraft was trimmed with the parameter shown in Table 3

Table 3 Trim variables

Trim variable	Value	Unit
V_T^*	69.1	ms^{-1}
θ^*	7.1	$^\circ$
α^*	7.1	$^\circ$
q^*	0	$rads^{-1}$
γ^*	0	rad

3.2.2 Small perturbation equations

Using these trim values, a linear state-space form of the equations was obtained using a third-order approximation based on the Taylor series expansion in [12] (p.199-202). This approximation is shown in Equation 13 and is a function of small perturbations (denoted by Δ) from the trim conditions.

$$\begin{bmatrix} \Delta \dot{V}_T \\ \Delta \dot{\theta} \\ \Delta \dot{\alpha} \\ \Delta \dot{q} \end{bmatrix} = \begin{bmatrix} -0.18 & -9.81 & -0.274 & 0 \\ 0 & 0 & 0 & 1 \\ -0.0041 & 0 & -0.59 & 1 \\ 0 & 0 & -0.26 & -0.15 \end{bmatrix} \begin{bmatrix} \Delta V_T \\ \Delta \theta \\ \Delta \alpha \\ \Delta q \end{bmatrix} + \begin{bmatrix} -0.001 & 9.85 \\ 0 & 0 \\ -0.00075 & -0.018 \\ -0.015 & 0 \end{bmatrix} \begin{bmatrix} \Delta \delta_e \\ \Delta \delta_t \end{bmatrix} \quad (14)$$

This approximation was verified by examining the eigenvalues of the A matrix which are $-0.40 \pm 0.45i$ and $0.022 \pm 0.17i$. As expected, these correspond to the two natural modes—the short-period and phugoid. Additionally, an open-loop throttle step response was examined. Figure 6 shows very good agreement between the nonlinear and linear model which verifies the approximation.

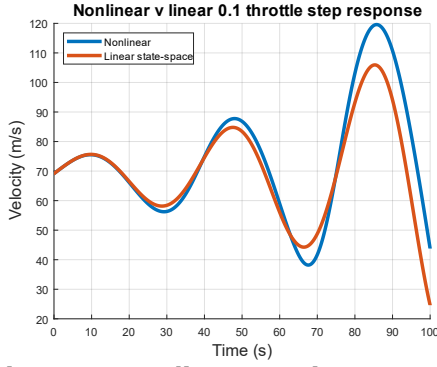


Figure 6 Nonlinear v Linear Open-Loop step response

3.3 Ship motion

The heaving and pitching of the ship is modelled by power spectral density functions $\Phi_H(s), \Phi_\theta(s)$ from [1]. These are transfer functions which output the ship motions given a white noise input. Equations 15 and 16 are the ones used here and represent a Forrestal-class carrier.

$$\Phi_H(s) = \frac{1.21}{s^4 + 2.08s^3 + 1.32s^2 + 0.4s + 0.16} \quad (15)$$

$$\Phi_\theta(s) = \frac{0.773s^2}{s^4 + 2.08s^3 + 1.32s^2 + 0.4s + 0.16} \quad (16)$$

Assuming the landing point (x_L, z_L) to be 81m from the centre of mass coordinates (x_G, z_G) [1], the combined landing point movement can be expressed as:

$$x_L = x_G - 81 \cos(\theta_s) \quad (17)$$

$$z_L = z_G - 81 \sin(\theta_s) \quad (18)$$

A power was not specified for the white noise in [1]. Hence, the power was tuned to match the maximum pitch and heave oscillation of 3° and 4m detailed in [15]. The power was set to -20Db and 4.5Db for the pitch and heave respectively. A typical landing point z-displacement can be seen in Figure 7

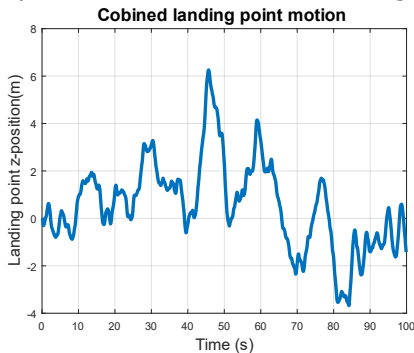


Figure 7 Landing point z-motion.

3.4 Wind

Based on the model detailed in the military specification [16], the x and z wind disturbances denoted by u_g, w_g contain 4

components. Free-air turbulence components and steady, periodic and random components of the carrier air wake. The free air turbulence (u_1, w_1) components were modelled by white-noise filters Φ_{u_1}, Φ_{w_1} similar to the power spectral density functions used in Equations 15 and 16

$$\Phi_{u_1} = \frac{200}{1 + (100s)^2} \quad (19)$$

$$\Phi_{w_1} = \frac{71.6}{1 + (100s)^2} \quad (20)$$

The air wake components were all given as functions of the carrier wind over deck $V_{w/d}$ which was assumed to be 10 m s^{-1} . Steady components (u_2, w_2) were presented as profiles, however, will be approximated as linear discontinuous functions of the distance X from the ships centre of pitch.

$$u_2 = \begin{cases} 0.002X, & 0 < X < 914\text{m} \\ 0, & X < 0 \end{cases} \quad (21)$$

$$w_2 = -1 + 0.0013X, \quad X < 914\text{m} \quad (22)$$

The periodic component was modelled as a function of ship pitch amplitude and frequency $\omega_p \theta_s$ which were approximated to be 1.25 rads^{-1} and 0.05 rad respectively based on outputs of Equation 15. The original formula also included the ship velocity which was assumed to be 0 m s^{-1} . Hence, the periodic components were calculated using Equations 23-25. The random components were omitted.

$$u_3 = \theta_s V_{w/d} (2.22 + 0.000091X) C \quad (23)$$

$$w_3 = \theta_s V_{w/d} (4.98 + 0.0018X) C \quad (24)$$

$$C = \cos\left(\omega_p \left[2.28t + \frac{X}{0.85V_{w/d}}\right] + 0.1\right) \quad (25)$$

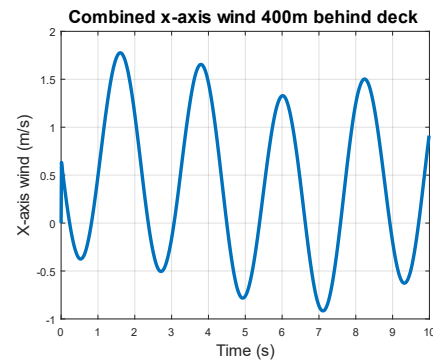


Figure 8 x-axis wind 400m behind deck

3.5 Noise

The pitch measurement noise was modelled by periodic component $0.001 \sin(7t)$ and a random component generated by the white noise generator in MATLAB using a power of -60Db.

3.6 Actuators

The actuators were modelled using first order filters. The engines and elevators were modelled with a 5 and 0.1 second lag respectively. These can be represented with the transfer functions shown below.

$$\text{Engine: } \frac{0.2}{s + 0.2} \quad \text{Elevator: } \frac{10}{s + 10}$$

3.7 Simulation

The system models were setup as systems of first order differential equations with known initial conditions, to form an initial value problem. Therefore, a Runge-Kutta 4th order algorithm was used to solve the system numerically. This algorithm was implemented in MATLAB. A time step of 0.001s was used to avoid numerical instabilities.

4 CONTROL ARCHITECTURE

4.1 Overview

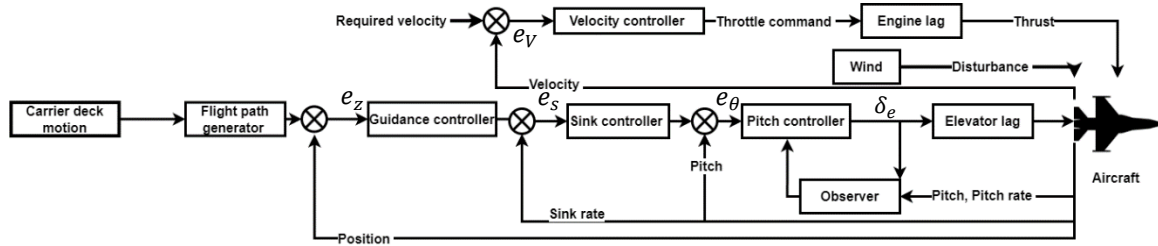


Figure 9 Control architecture

As shown in Figure 9 the architecture used will be based on the original architecture described in section 2.1. A flight path generator projects an ideal flight path from the landing position. A position error between the ideal flight path and aircraft is determined and fed into a guidance controller which outputs a required sink rate. This sink rate is fed into a sink controller which outputs a required pitch angle. This command is executed by the pitch controller which sends a control signal to the elevators. Meanwhile, the velocity controller maintains a constant airspeed. The observer uses feedback from the aircraft and the pitch controller, to estimate the disturbance and improve control performance.

4.2 Pitch controller

The pitch controller is designed to track a reference pitch command by controlling the elevator. By observing the disruptions and nonlinearities in a combined disturbance, a linear controller can be used to achieve the desired performance.

4.2.1 Observer

Based on equations 2 and 4 and the linearisation 14 the equation of motion for the pitch dynamics is 25:

$$\Delta\ddot{\theta} = \frac{\partial\dot{q}}{\partial q}\Delta\dot{\theta} + \frac{\partial\dot{q}}{\partial\delta_e}\Delta\delta_e + \frac{\partial\dot{q}}{\partial\alpha}\Delta\alpha \quad (26)$$

This can be rearranged in terms of a known input $h_\theta(t)$ and unknown disturbance $d_\theta(t)$ with derivative $\eta_\theta(t)$. Where $d_\theta(t)$ Represents all the combined disturbances, from neglected terms, noise and nonlinear dynamics omitted in the linear approximation.

$$\Delta\ddot{\theta} = h_\theta(t) + d_\theta(t) \quad (27)$$

$$h_\theta(t) = \frac{\partial\dot{q}}{\partial q}\Delta\dot{\theta} + \frac{\partial\dot{q}}{\partial\delta_e}\Delta\delta_e \quad (28)$$

Hence the equations are in an appropriate form required by the observer and detailed by Equations 7-10 with $y_{op} = \Delta\theta$. Hence, Equations 11-13 can be used to estimate the pitch angle perturbation, pitch rate and disturbance denoted by $\widehat{\Delta\theta}, \widehat{\Delta\dot{\theta}}, \widehat{d}_\theta$ with x_1, x_2, x_3 respectively.

4.2.2 Controller

By defining error as

$$e_\theta = \theta_r - \theta = \Delta\theta_r - \Delta\theta, \dot{e}_\theta = -\Delta\dot{\theta} \quad \ddot{e}_\theta = -\Delta\ddot{\theta}$$

And using equation 25, 26 and 27 the error system becomes

$$\ddot{e}_\theta - \frac{\partial\dot{q}}{\partial q}\dot{e}_\theta = -\frac{\partial\dot{q}}{\partial\delta_e}\Delta\delta_e - d_\theta(t) = -U_{e\theta}(t) \quad (29)$$

Where $U_{e\theta}(t)$ is an equivalent controller selected as a proportional derivative controller

$$U_{e\theta}(t) = K_{P\theta}e_\theta(t) + K_{D\theta}\dot{e}_\theta \quad (30)$$

Hence the characteristic equation can be expressed by

$$s^2 + \left(K_{D\theta} + \frac{\partial \dot{q}}{\partial q} \right) s + K_{P\theta} = 0 \quad (31)$$

This second order error system can be expressed in terms of natural frequency ω_n and damping ratio γ_1 which can be selected to achieve the desired system performance:

$$s^2 + 2\gamma_1\omega_n s + \omega_n^2 = 0 \quad (32)$$

$$K_{IV} = K_{P\theta}, \quad K_{D\theta} = 2\gamma_1\omega_n - \frac{\partial \dot{q}}{\partial q} \quad (33)$$

The natural frequency can be expressed in terms of the convergence time to reach 2% of the required value $T_{2\%}$

$$\omega_n = \frac{4}{T_{2\%}\gamma} \quad (34)$$

The damping ratio was selected as $\sqrt{2}$ to speed up convergence. The desired settling time was reduced to 0.3s until there was no improvement in performance shown by the simulated convergence time. The controller parameters used are shown below.

$$K_{D\theta} = 26.5186 \quad K_{P\theta} = 88.89$$

Although the disturbance is unmeasurable, an observer estimate can be used instead making all variables in the equation known. Therefore, the equivalent controller and disturbance estimate can be used to determine the change in elevator deflection as follows:

$$\Delta \delta_e = \frac{U_{e\theta}(t) - \widehat{d}_\theta(t)}{\frac{\partial \dot{q}}{\partial \delta_e}} \quad (35)$$

The final elevator deflection can be determined as by summing the elevator perturbation with the trimmed value as.

$$\delta_e = \delta_e^* + \Delta \delta_e \quad (36)$$

4.2.3 PID for comparison

A Proportional Integral Derivative PID pitch controller has also been implemented for comparison. The PID equivalent controller can be expressed as

$$U_{e\theta 2}(t) = K_{P\theta 2}e_\theta(t) + K_{I\theta} \int_0^t e_s(\tau) d\tau + K_{D\theta 2}\dot{e}_\theta \quad (37)$$

With the controller parameters shown below

$$K_{P\theta 2} = 57.01 \quad K_{I\theta} = 50 \quad K_{D\theta 2} = 17.19$$

4.3 Velocity controller

The velocity controller is designed to maintain a constant velocity by controlling the engine thrust. Due to the relatively low coupling between the airspeed and other parameters,

the velocity controller can be designed directly. Defining the error assuming constant reference.

$$e_V = V_R - V_T, \quad \dot{e}_V = -\dot{V}_T$$

Based on Equation 1 the error system becomes:

$$\dot{e}_V = \dot{V}_R - \frac{T \cos(\alpha)}{m} + \frac{D}{m} + g \sin(\gamma) \quad (38)$$

By assuming small angles and grouping the other state variables into a combined disturbance d_v the error system becomes:

$$\dot{e}_V = -\frac{T}{m} + d_v(t) = -U_{eV}(t) \quad (39)$$

Selecting the equivalent controller such that the error system becomes an autonomously stable system with the ability of rejecting unknown constant disturbance. A PID controller is selected.

$$U_{eV}(t) = K_{DV}\dot{e}_V(t) + K_{PV}e_V(t) + K_{IV} \int_0^t e_V(\tau) d\tau \quad (40)$$

Hence, the characteristic equation becomes.

$$s^2(1 + K_{DV}) + K_{PV}s + K_{IV} = 0 \quad (41)$$

Once the equivalent controller is calculated from the error terms, the actual thrust command can be determined as follows:

$$T = m(U_{eV}(t)) \quad (42)$$

4.4 Sink controller.

The sink controller is responsible for controlling the aircrafts rate of descent (sink rate) \dot{z} by inputting a sink rate error e_s and outputting a required pitch angle θ_R . Due to the coupled nature of the equations of motion, a fixed relationship between the pitch and sink rate is difficult to obtain as it also depends on the other state variables. Hence, a proportional integral (PI) controller was applied directly and tuned manually until an acceptable performance was achieved. Defining the error as $e_s = \dot{z}_R - \dot{z}$ The sink controller can be expressed as

$$\theta_R(t) = K_{PS}e_s + K_{IS} \int_0^t e_s(\tau) d\tau \quad (43)$$

Where the controller parameters were selected as

$$K_{PS} = 0.0061 \quad K_{IS} = 0.018$$

4.5 Guidance controller

The guidance controller takes the vertical deviation e_z and outputs a sink rate command \dot{z}_R . Similarly, to the sink rate controller, a PID controller was applied directly and tuned

manually. Defining the error as $e_z = z_R - z$ the controller can be expressed as:

$$\dot{z}_R(t) = K_{Pz}e_z + K_{Iz} \int_0^t e_z(\tau)d\tau + K_{Dz}\dot{e}_z(t) \quad (44)$$

Where the controller parameters are selected as:

$$K_{Pz} = 1 \quad K_{Iz} = 0.5 \quad K_{Dz} = 0.01$$

5 RESULTS

Figure 10, Figure 11 and Figure 12 show the performance of Observer based Proportional Derivative (O-PD) controller vs the PID controller. In near ideal conditions, where there is no additional noise or wind, both controllers converge to the required value under 3 seconds.

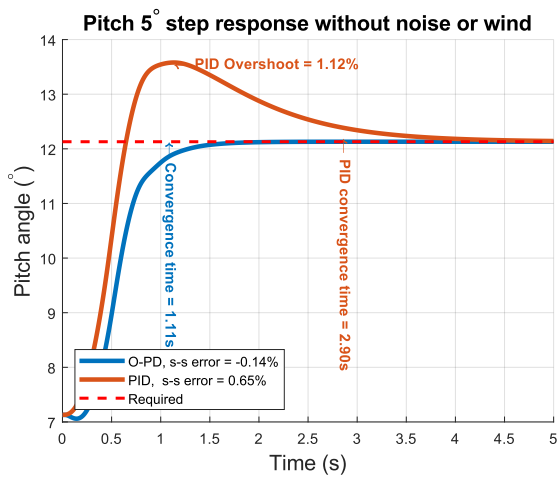


Figure 10 Pitch step response without noise or wind

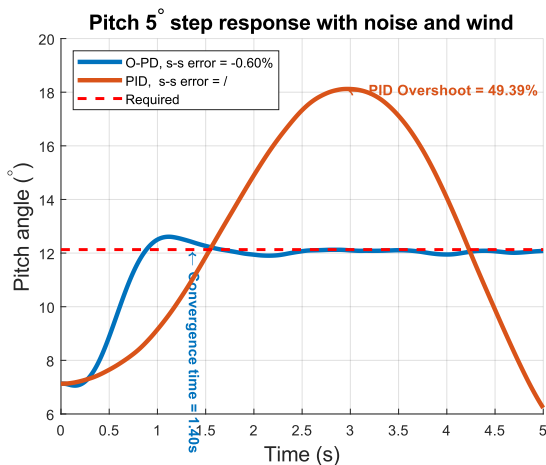


Figure 11 Pitch step response with noise and wind

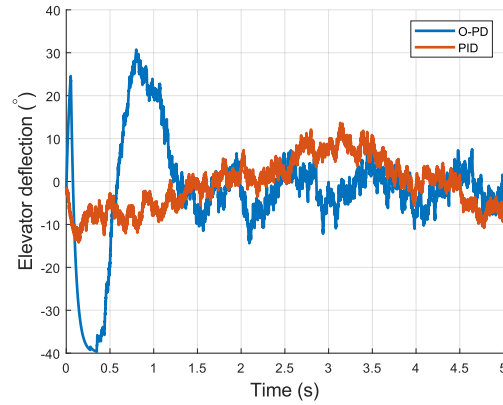


Figure 12 Elevator deflection during step response with noise and wind

As shown by Figure 10, although the steady-state (s-s) error is under 1% for both controllers, the O-PD controller converges in 1.11s, 85% faster than the PID controller. In the adverse case, with both noise and wind present as shown in Figure 11, the PID completely fails to stabilise the pitch dynamics, whereas the O-PD converges to within 2% of the required value within 1.4s which is 26% slower than in the ideal case. Figure 13 shows the sink rate error and trajectory of the aircraft when tracking a constant sink rate of 10 ms^{-1} . The sink-controller to O-PD is shown to be adequate, converging to the required value within 0.5s with negligible steady-state error.

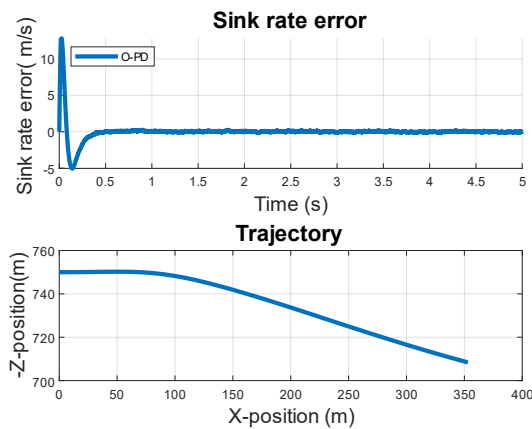


Figure 13 Sink rate error and trajectory for a constant required sink rate

The position error between the aircraft and the ideal glide does not converge to 0 as shown in Figure 14. The sink and pitch controllers were shown to perform well; hence, the guidance controller or guidance-sink controller coupling is the most likely source of the problem and should be investigated in further work. Potentially, re-tuning might improve performance. Figure 15 shows that O-PD controller tracks the highly time-varying required value. This highlights the good performance of the O-PD.

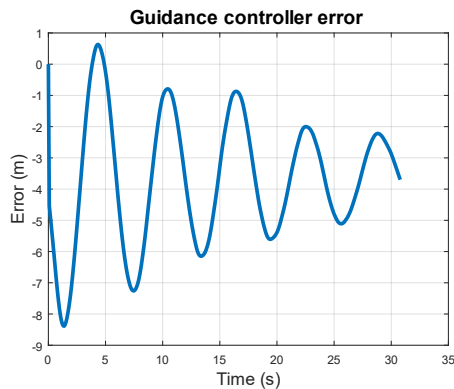


Figure 14 Position error approaching carrier.

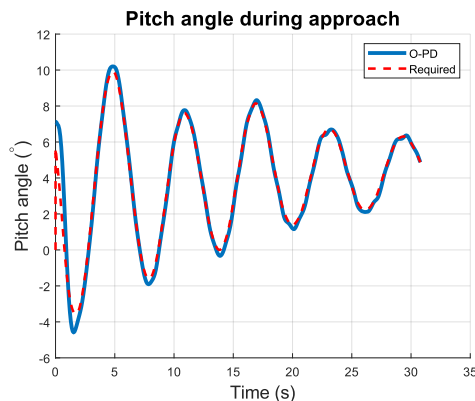


Figure 15 Pitch angle response on approach

6 FURTHER WORK

As non-linear observer has been shown to be effective at controlling the pitch dynamics, further work could be done to apply similar methods for the roll and yaw dynamics and control the full 6 degree-of-freedom equation of motions. Based on this study, a PID guidance controller does not seem effective at controlling the trajectory in a suitable way for carrier landing. Hence, more work could be done to combine the designed pitch controller with better guidance methodologies. Assuming alternative guidance approaches to be effective, the effect of measurement delay and ways to mitigate it could be considered in the carrier landing context.

7 CONCLUSION

Carrier landings are difficult to control due to nonlinear dynamics, wind disturbances, measurement noise and a highly time-varying trajectory. A numerical model of an F/A-18 and adverse conditions based on previous research has been developed and implemented in MATLAB software. A nonlinear observer was used to estimate a combined disturbance in the pitch dynamics. Together with a PD controller, this estimate was used to achieve satisfactory pitch control performance. In ideal conditions, the controller was shown to

converge 85% faster than a PID controller with little overshoot. Additionally, the controller was shown to robustly track a time-varying reference in the presence of wind disturbances and noise. Together with a PI sink controller, the control system was shown to converge to a constant required sink rate in under 1s. However, when combined with a guidance controller, the performance was inadequate. Hence, further work should focus on applying the O-PD controller to the roll and yaw dynamics and combining with a better guidance and sink controller.

8 REFERENCES

- [1] T. S. Durand and G. L. Teper, "AN ANALYSIS OF TERMINAL FLIGHT PATH CONTROL IN CARRIER LANDING," SYSTEMS TECHNOLOGY, INC., Inglewood, California, 1964.
- [2] T. Robinson, "MQ-25 - the future of carrier aviation?," Royal Aeronautical Society, 12 July 2022. [Online]. [Accessed December 2022].
- [3] X. Wang and B. Shirinzadeh, "Nonlinear augmented observer design and application to quadrotor aircraft," *Nonlinear Dynamics*, 2015.
- [4] P. FITZGERALD, *FLIGHT CONTROL SYSTEM DESIGN FOR AUTONOMOUS UAV CARRIER LANDING*, Cranfield university, 2004.
- [5] J. M. Urnes and R. K. Hess, "Development of the F/A-18A Automatic Carrier Landing system," *Journal of Guidance, Control, and Dynamics*, vol. 8, no. 3, 1985.
- [6] L. Yue, G. Liu and G. Hong, "Design and Simulation of F/A-18A Automatic Carrier Landing Guidance Controller," in *AIAA Modeling and Simulation Technologies Conference*, Washington D.C., 2016.
- [7] L. Wang, Z. Zhang, Q. Zhu and Z. Wen, "Design of Automatic Carrier-Landing Controller Based on Compensating States and Dynamic Inversion," *IEEE Access*, 2019.
- [8] S. Lee, J. Lee, S. Lee, H. Choi and Y. Kim, "Sliding Mode Guidance and Control for UAV carrier landing," *IEEE TRANSACTIONS ON AEROSPACE AND ELECTRONIC SYSTEMS*, vol. 55, no. 2, 2019.
- [9] Z. Zhen, S. Jiang and K. Ma, "Automatic carrier landing control for unmanned aerial vehicles based on preview control and particle filtering," *Aerospace Science and Technology*, no. 81, pp. 99-107, 2018.
- [10] K. Cui, W. Han, Y. Liu, X. Wang, X. Su and J. Liu, "Model Predictive Control for Automatic Carrier Landing with Time Delay," *International Journal of Aerospace Engineering*, vol. 2021, 2021.
- [11] Z. Sun, L. Wu, and Y. You. "Automatic Landing System Design for Unmanned Fixed-Wing Vehicles via Multivariable Active Disturbance Rejection Control." *Int. J. Aerosp. Eng.*, 2023.
- [12] B. L. Stevens, F. L. Lewis and E. N. Johnson, *Aircraft Control And Simulation*, Hoboken: John Wiley & Sons, Inc, 2016.
- [13] N. Ananthkrishnan and N. K. Sinha, *Elementary Flight Dynamics with an Introduction to Bifurcation and Continuation Methods*, Boca Raton : Taylor & Francis Group, LLC, 2013.
- [14] NASA, Dryden Flight Research Centre, "Documentation for a Dynamic Inversion Control Law Proposed for RFCs," [Online]. Available: <https://www.nasa.gov/centers/dryden/history/pastprojects/HARV/WorK/NASA2/nasa2.html>.
- [15] W. A. Johnson, "ANALYSIS OF AIRCRAFT CARRIER MOTIONS IN A HIGH SEA STATE," SYSTEMS TECHNOLOGY. INC., Hawthorne, California 90250, 1969.
- [16] D. J. Moorhouse and R. J. Woodcock, "BACKGROUND INFORMATION AND USER GUIDE FOR MIL-F-8785C, MILITARY SPECIFICATION FLYING QUALITIES OF PILOTED AIRPLANES," FLIGHT DYNAMICS LABORATORY AIR FORCE WRIGHT AERONAUTICAL LABORATORIES AIR FORCE SYSTEMS COMMAND WRIGHT-PATERSON AIR FORCE BASE,, Ohio, 1982.